Mitigating the optical depth degeneracy in the cosmological measurement of neutrino masses using 21-cm observations

Gali Shmueli[*] Debanjan Sarkar[†] and Ely D. Kovetz[‡]

Department of Physics, Ben-Gurion University Be'er Sheva 84105, Israel

Massive neutrinos modify the expansion history of the universe and suppress the structure formation below their free streaming scale. Cosmic microwave background (CMB) observations at small angular scales can be used to constrain the total mass Σm_ν of the three neutrino flavors. However, at these scales, the CMB-measured Σm_ν is degenerate with τ, the optical depth to reionization, which quantifies the damping of CMB anisotropies due to the scattering of CMB photons with free electrons along the line of sight. Here we revisit the idea to use 21-cm power spectrum observations to provide direct estimates for τ. A joint analysis of CMB and 21-cm data can alleviate the $\tau - \Sigma m_\nu$ degeneracy, making it possible to measure Σm_ν with unprecedented precision. Forecasting for the upcoming Hydrogen Epoch of Reionization Array (HERA), we find that a $\lesssim \mathcal{O}(10\%)$ measurement of τ is achievable, which would enable a $\gtrsim 5\sigma$ measurement of $\Sigma m_\nu = 60$ [meV], for any astrophysics model that we considered. Precise estimates of τ also help reduce uncertainties in other cosmological parameters, such as A_s, the amplitude of the primordial scalar fluctuations power spectrum.

I. INTRODUCTION

Since its discovery, the cosmic microwave background (CMB) [1] has played a dominant role in our understanding of the Universe. Observing the CMB allows us to learn more about the origins and evolution of the universe, and test our current understanding of fundamental physics [2–10]. One such example is the measurement of the sum of neutrino masses $\sum m_\nu$. Neutrinos come in three flavors. Neutrino oscillation experiments have revealed that neutrinos have mass and obey three possible hierarchies: normal, inverted, and degenerate [11–18]. Due to their nonzero mass, neutrinos contribute to the total energy density of the Universe and affect the cosmic expansion rate and evolution of cosmic structures [19–22]. This renders the CMB and large-scale structure sensitive probes of the sum of neutrino masses [23–38].

However, processes in the late time universe, like the epoch of reionization (EoR) [39,40], limit the precision with which we can measure neutrino masses. Free electrons along the light of sight to the surface of last scattering influence the CMB anisotropies, an effect characterized by the parameter τ—known as the optical depth to reionization [41]—which is one of the six parameters of the ΛCDM. It has two main effects on the CMB power spectra [42,43].

First, it damps the scalar perturbations as generated at recombination by a factor $\exp(-2\tau)$. This makes it highly degenerate with A_s, the amplitude of the primordial scalar perturbations, and at high multipoles, or smaller scales, also highly degenerate with the sum of neutrino masses $\sum m_\nu$ [44]. Second, the rescattering of the CMB photons off free electrons at the reionization epoch generates a bump in the CMB polarization power spectra at large angular scales [45,46]. Observation of the large-scale CMB polarization thus provides a measurement of τ, which allows breaking the degeneracy with A_s and $\sum m_\nu$ to some extent. Improving the measurement of τ will be crucial for differentiating between the mass hierarchies of neutrinos and enabling a robust detection of the total mass.

A number of current probes, including the Lyman-α forest [47–49], Lyman-α emitting galaxies [50–53], the kinematic Sunyaev-Zeldovich effect [54–58], etc., allow to place direct constraints on τ. Similarly, $\sum m_\nu$ can also be determined by measuring the expansion rate using distance ladders [59,60], from large-scale structure surveys [33,61–63], Lyman-α forest surveys [64,65], line-intensity mapping [66–68], the post-reionization 21-cm signal [69–75], etc. All these independent observations can be combined together for a precision measurement of $\sum m_\nu$. In this paper, we assess the feasibility of using the 21-cm signal from EoR as a direct probe of τ.

The redshifted 21-cm observations are a very sensitive probe of EoR. A number of telescopes such as LOFAR [76], HERA [77], GMRT [78] and SKA [79] are seeking

---
[*]shmugal@post.bgu.ac.il
[†]debanjan@post.bgu.ac.il
[‡]kovetz@bgu.ac.il

the signal from high redshifts. Fluctuations in the 21-cm signal probe the density-weighted electron fraction in the EoR, which is the primary ingredient required to compute τ. Therefore, 21-cm observations provide an independent measurement of τ [80–82]. Small-scale damping in the 21-cm power spectrum, caused by the neutrinos, also provides an independent estimate of $\sum m_\nu$ [83]. A joint analysis of the 21-cm fluctuations and the CMB data thus helps to precisely estimate τ, break the $\tau - \sum m_\nu$ degeneracy, and significantly reduce $\Delta \sum m_\nu$. This idea was first coined by Ref. [81] where it was shown that $\Delta \sum m_\nu$ can be measured with ± 12 [meV] accuracy if 21-cm observations from HERA are combined with the CMB observations. Here we revisit the analysis presented in Ref. [81] with an updated treatment and provide forecasts for the combination of HERA and the planned CMB-S4 experiment [84,85].

In order to generate the mock observations of HERA, Ref. [81] used the publicly available code 21cmFAST[1] which assumes an inside-out model of reionization based on the excursion set formalism as described in Ref. [86]. However, since their analysis, the 21cmFAST code has been augmented with improved modeling (involving new parametrization) of the cosmic dawn and reionization astrophysics [87–89]. Furthermore, for simplicity, they assumed throughout the calculation that the spin temperature, T_S, is much higher than the CMB temperature, T_{CMB} ($T_S \gg T_{CMB}$), which is true only at the very advanced stages of reionization. In addition, they assumed an observation from HERA spanning a limited redshift range of $6.1 \leq z \leq 9.1$.

In the analysis presented below, we use the latest version of the 21cmFAST code, relax the assumption $T_S \gg T_{CMB}$, accounting for the exact evolution of T_S, T_{CMB} and the kinetic temperature T_K as computed by the 21cmFAST code, and consider 21-cm observations from HERA across the redshift range $5 \leq z \leq 27$, which spans the cosmic-dawn (CD) era down to the end of reionization. We have further considered additional effects like the Lyman-α heating of the inter-galactic medium[2] [90–94], Population III stars[3] [88,89,95–97], the relative velocity between dark matter and baryon fluid[4] [100–106], and

in-homogeneous Lyman-Werner (LW) radiation feedback[5] [108–113]. Note that, in the current public version of the 21cmFAST code, the Lyman-α heating is not included. We have made necessary changes in the code to accommodate the Lyman-α heating in our calculations [114]. Further, we have interfaced 21cmFAST with the public Boltzmann code CLASS[6] [115–118] so that the cosmological and astrophysical parameter degeneracies can be studied consistently in a joint analysis of the CMB and 21-cm signals. For more details on our implementation, the reader is referred to Refs. [114,119].

Using Fisher-based forecasts, we demonstrate that the combination of 21-cm and CMB data from HERA and CMB-S4 can yield a measurement of $\sum m_\nu$ beyond the precision required for a robust determination of the neutrino mass hierarchy and a greater than 5σ detection of the minimal sum of neutrino masses.

This paper is structured as follows. In Sec. II, we describe the fiducial experiments and observables used in our analysis, and present in detail the methodology used in this work. In Secs. III and IV we present our results, and in Sec. V we summarize our main findings.

II. FORMALISM

In this section, we discuss the fiducial experiments we chose to consider, along with the various observables as well as the assumptions made throughout the analysis.

A. CMB

For the CMB experiments, we mainly used the publicly available data products from *Planck*-2018 data release [120,121]. We focus on the "TT, TE, EE + LowE+ Lensing + BAO" dataset since it provides the tightest errors on parameters. We use the best-fit values from this dataset as our fiducial cosmological parameters, and use the covariance matrices provided by the *Planck* collaboration.[7] For simplicity, we assume Gaussian parameter uncertainties so that the inverse of the covariance matrix gives us the Fisher matrix which we require later in the analysis. More details are given in Appendix A.

---

[1]https://github.com/21cmfast/21cmFAST.

[2]This mechanism is due to the resonant scattering between Lyman-α photons and the IGM atoms, and is important when the x-ray heating efficiency is not very high.

[3]These first generations of stars are assumed to have formed inside *mini* halos, in the mass range 10^5–$10^6 M_\odot$, where the molecular cooling process makes star formation possible in those halos.

[4]This supersonic relative velocity between dark matter and baryons after recombination is generated due to the interaction between baryons and photons before recombination. The same interaction gives rise to the baryon acoustic oscillations. This supersonic velocity applies negative feedback and hinders structure formation inside the minihalos, modulating star-formation on large scales. [88,98,99].

[5]The UV photons in the Lyman-Werner band (11.2–13.6 eV) photo-dissociate the molecular hydrogen and imposes negative feedback on star formation. In an earlier work, Ref. [107] have implemented the LW radiation feedback for the 21-cm calculations in the 21cmFAST code. This work, however, assumed that the intensity of LW radiation does not vary spatially, which is physically less plausible. In a recent work, Ref. [89] has updated the calculations to include the spatial variation of the LW radiation intensity in the latest version of the 21cmFAST code.

[6]https://github.com/lesgourg/class_public.

[7]https://wiki.cosmos.esa.int/planck-legacy-archive/index.php/Cosmological_Parameters.

B. 21-cm observations

Next, we consider radio-interferometer observations of the redshifted 21-cm signal from the neutral hydrogen (HI). These measure the Fourier transform of the two-point correlation function of the intensity fluctuations, also known as the power spectrum

$$\Delta_{21}^2(k, z) = \frac{k^3 P_{21}(k, z)}{2\pi^2} \qquad (1)$$

where $P_{21}(k, z) = \langle \tilde{T}_{21}(\vec{k}, z) \tilde{T}_{21}^*(\vec{k}, z) \rangle$ and $\tilde{T}_{21}(\vec{k}, z)$ is the Fourier transform of $T_{21}(\vec{x}, z) - \langle T_{21}(z) \rangle$. Here $T_{21}(\vec{x}, z)$ represents the 21-cm intensity fluctuations from various positions and directions in the sky, and $\langle T_{21}(z) \rangle$ is the sky average of the intensity fluctuations at a single redshift. $T_{21}(\vec{x}, z)$ can be approximately written as [122–124],

$$T_{21}(\vec{x}, z) \approx T_0 x_{\rm HI}(1 + \delta_b)\left(1 - \frac{T_{\rm CMB}}{T_s}\right)\left(\frac{H}{H + \partial v_r/\partial r}\right), \quad (2)$$

where $x_{\rm HI}$ is the hydrogen neutral fraction, δ_b is the baryon density contrast, $T_{\rm CMB}$ is the temperature of the CMB, T_s is the spin temperature of the hydrogen atoms, $\partial v_r/\partial r$ is the derivative of the comoving radial peculiar velocity with respect to the comoving radial distance and T_0 being,

$$T_0 = \frac{9\hbar c^2 A_{10}\Omega_b H_0}{128\pi G k_B \nu_{21}^2 \mu m_p \Omega_m^{1/2}}\left(1 - \frac{Y_p^{\rm BBN}}{4}\right) \qquad (3)$$

where $\hbar$ is Planck's constant, $A_{10} = 2.86 \times 10^{-15} \text{ s}^{-1}$ is the Einstein coefficient for the hyperfine (21-cm) transition, G is the gravitational constant, k_B is Boltmann's constant, $\nu_{21} \approx 1420$ MHz is the frequency of the 21-cm line, m_p is the proton mass, H_0 is the Hubble parameter, Ω_b is the normalized baryon energy density, Ω_m is the normalized matter density, $Y_p^{\rm BBN}$ is the helium abundance and μ is the mean molecular weight. On large scales, δ_b can be approximately assumed to be the same as the dark matter overdensity δ_m which is a crucial assumption in the seminumerical simulations. In the inside-out model of reionization, sources form at the high density (or high δ_m) regions and the ionizing photons propagate out of those regions to ionize H I. Therefore, the regions around the high densities are highly ionized with $x_{\rm HI} \approx 0$. On the other hand, the low density regions keep the hydrogen neutral ($x_{\rm HI} \approx 1$) until the end of reionization. These low density regions contribute to the 21-cm signal budget at high redshift. Further, baryons in these low-density regions directly follow the dark matter distribution, so that assumption $\delta_b = \delta_m$ holds.

In order to simulate the observed 21-cm power spectrum and global signal for an input set of astrophysical and cosmological parameters, we use a modified version of the public semi-numerical code 21cmFAST [89],[8] used by Refs. [114,119], that includes the effects of Lyman-α. This code is also interfaced with the CLASS code so that the degeneracies of the cosmological parameters can be robustly studied. Once again, for more information about the various features used in our code, the reader is referred to Refs. [114,119]. The astrophysical parameters and modeling we used are elaborated on in Refs. [88,89].

We have considered three different configurations of the 21cmFAST code in calculating our results:

(i) Scenario A: Here we assume that both the Population II stars (formed inside the halos that contain atomic-cooling galaxies or ACGs[9]) and Population III stars (formed inside mini-halos containing molecular-cooling galaxies MCGs[10]) are present in the simulations. The presence of Population III prepones the onset of cosmic dawn, which otherwise would occur at a later time [88,89]. Population III stars affect the evolution of the 21-cm signal significantly, as can be seen in various recent works [100–107]. In Table I, we mention some of the main astrophysical parameters used in this work.

(ii) Scenario B: Here we do not consider the contribution from MCGs, retaining only ACGs in the simulations.

(iii) Scenario C: In this case, we adopt the old parametrization of the 21cmFAST code as was done in Ref. [81]. Following Ref. [81], we use three parameters to parametrize the reionization process: $T_{\rm vir}$, the minimum virial temperature of the first ionizing galaxies; ζ, the ionizing efficiency of those galaxies; and $R_{\rm mfp}$, the mean free path of ionizing photons in ionized regions in the Universe. This lets us compare our estimates directly with the findings of Ref. [81]. This old parametrization, like in Scenario B, includes only ACGs. However, note that we can only compare our results qualitatively with Ref. [81] as we are using the latest version of the 21cmFAST code where some calculations have been updated.

It is important to note that, Scenario A is believed to represent the most updated prescription of astrophysics at high redshifts, and we shall mainly focus on Scenario A when presenting our results. Meanwhile, Scenario B and Scenario C will be considered as two alternative simple prescriptions to be used for comparison.

For all three scenarios, we run the 21cmFAST code with a box size of 600 Mpc and 1 Mpc resolution to compute the 21-cm global signal and fluctuations. We drop the

---

[8]https://github.com/debanjan-cosmo/21cmFAST/tree/21cmFAST-heating.

[9]ACGs mainly obtained their gas through H I (and He) line transitions that are efficient at virial temperatures $T_{\rm vir} \gtrsim 10^4$ K.

[10]Inside MCGs, the gas cools mainly through the H_2 rotational–vibrational transitions efficient at $T_{\rm vir} \sim 10^3$–10^4 K. Note that, most ACGs at high redshifts are "second-generation" galaxies, forming out of MCGs.

TABLE I. The main astrophysics parameters and their definitions used in Scenario A and Scenario B (refer to Sec. II B).

Parameters	Description
$f_{\star,10}$ ·······	Stellar to halo mass ratio at $M_{\rm vir} = 10^{10} M_\odot$ for ACGs
$f_{\star,7}$ ········	Stellar to halo mass ratio at $M_{\rm vir} = 10^7 M_\odot$ for MCGs
$f_{\rm esc,10}$ ·····	Escape fraction of ionizing photons at $M_{\rm vir} = 10^{10} M_\odot$ for ACGs
$f_{\rm esc,7}$ ·······	Escape fraction of ionizing photons at $M_{\rm vir} = 10^7 M_\odot$ for MCGs
L_X ·········	Soft-band x-ray luminosity per SFR in units of $\mathrm{erg\,s^{-1}\,M_\odot^{-1}\,yr}$ for ACGs
$L_{X,\rm mini}$ ·····	Soft-band x-ray luminosity per SFR in units of $\mathrm{erg\,s^{-1}\,M_\odot^{-1}\,yr}$ for MCGs

assumption $T_S \gg T_{\rm CMB}$ used in Ref. [81] and consider the exact evolution of the temperatures as given by 21cmFAST. We also consider the Lyman-α heating, the relative velocity between dark matter and baryon, and regular LW radiation feedback strength (as defined in Ref. [89]) for all the simulations. Note that, the relative velocity and the LW feedback mostly affect the MCGs. We, therefore, expect to see the signatures of these effects only in Scenario A.

We make forecasts for the HERA 21-cm intensity mapping experiment [77]. HERA will measure the 21-cm fluctuations from Cosmic Dawn (50 MHz or $z \sim 27$) to the reionization era (225 MHz or $z \sim 5$). The ultimate setup of HERA is expected to contain 350 antenna dishes, each with a diameter of 14 m. Out of the 350 dishes, 320 will be placed in a close-packed hexagonal configuration and the remaining 30 will be placed at longer baselines. We calculate the sensitivity of the HERA observations using the publicly available package 21 CMSENSE[11] [125,126]. This code accounts for the $u - v$ sensitivities of each antenna in the array and calculates the possible errors in the 21-cm power spectrum measurement, including cosmic variance. The total redshift coverage of HERA is divided into 30 bins, and we assume that all the redshift bins are observed simultaneously for a total of 180 days with 6 hours of observation per day. For the receiver temperature we take $T_{\rm rec} = 100$ K.

In the 21-cm observations, the foreground is many orders of magnitude brighter than the signal and is anticipated to contaminate a significant amount of Fourier space [127–130]. In the $k_\perp - k_\parallel$ space, where $k_\parallel$ and $k_\perp$ are the components of the wave vector respectively parallel and perpendicular to the line-of-sight direction, the contaminated part of the Fourier space appears like a "wedge" [126,131]. The extent of this foreground wedge can be parametrized [125,126] by assuming that all wave numbers with $k_\parallel$ below

$$k_\parallel^{\min} = a + b(z)k_\perp,$$

are contaminated, where $b(z)$ accounts for the chromaticity of the antennae, and a is a constant superhorizon buffer.

[11]github.com/steven-murray/21cmSense.

In this paper, we consider "moderate" foreground contamination (as defined in Refs. [125,126]) in 21CMSENSE for the 21-cm observations with HERA. Here we assume $b(z)$ is determined by the horizon limit, and consider $a = 0.05\,h\,{\rm Mpc}^{-1}$. Further, the baselines are added coherently. For a comprehensive reading about the details of the different setups and foreground scenarios, the reader is referred to Refs. [125,126].

C. Optical depth calculation

The optical depth to reionization, τ, is one of the six parameters of the concordance ΛCDM model of cosmology, and is given by the line-of-sight integration of the mean electron density $\overline{n_e}$

$$\tau = \sigma_T \int \overline{n_e}(z) \frac{dl}{dz} dz, \tag{4}$$

where σ_T is the Thompson cross-section, and $\frac{dl}{dz}$ is the proper line-of-sight distance per unit redshift. The mean electron density $\overline{n_e}(z)$ can be explicitly calculated using,

$$\overline{n_e} = \overline{n_b}\left[\overline{x_{\rm HII}(1 + \delta_b)} + \frac{1}{4}\overline{x_{\rm HeIII}(1 + \delta_b)} Y_p^{\rm BBN} \right], \tag{5}$$

where $n_b = n_{\rm H} + n_{\rm He}$ is the baryon number density, which in turn is the sum of the hydrogen $n_{\rm H}$ and helium $n_{\rm He}$ number densities. The ionization fractions (defined to be between 0 and 1) are given by $x_{\rm HII}$, and $x_{\rm HeIII}$, referring to singly ionized hydrogen and doubly ionized helium, respectively. The helium fraction $Y_p^{\rm BBN}$ is defined as $4n_{\rm He}/n_b$, and δ_b denotes the baryon overdensity. Assuming the uncertainties in the helium reionization to be negligible, as in Ref. [81], and that helium is instantaneously reionized at $z = 3$, the expression for the optical depth sourced by free electrons from HI/HeI reionization (neglecting the contribution from HeII reionization), can be simplified as,

$$\tau = \frac{3H_0 \Omega_b \sigma_T c}{8\pi G m_p} \left[1 + \frac{Y_p^{\rm BBN}}{4} \left(\frac{m_{\rm He}}{m_{\rm H}} - 1 \right) \right]^{-1}$$
$$\times \int_0^{z_{\rm CMB}} \frac{dz(1 + z)^2}{\sqrt{\Omega_\Lambda + \Omega_m(1 + z)^3}} \overline{x_{\rm HII}(1 + \delta_b)} \tag{6}$$

Note that, except for the $\overline{x_{\mathrm{HII}}.(1+\delta_b)}$ term, which is the density-weighted ionization fraction [and is not equal to $\overline{x_{\mathrm{HII}}}.(1+\delta_b)$], all the other terms are either fundamental constants or cosmological parameters constrained by Planck and other observations. These measurements of the cosmological parameters come with their own uncertainties, which introduces errors in the calculation of τ.

So, for the time being, let us focus on this $\overline{x_{\mathrm{HII}}.(1+\delta_b)}$ term. Due to the presence of $(1+\delta_b)$, it is not straightforward to calculate $\overline{x_{\mathrm{HII}}(1+\delta_b)}$. However, we can guess its values at certain redshifts. For example, at $z < 5$, where the universe is almost completely ionized, we can approximately take $\overline{x_{\mathrm{HII}}(1+\delta_b)} \approx 1$, which makes the integration utterly simple in this z range. Meanwhile, at high redshifts (preceding reionization) we do not have sufficient free electrons, and so $\overline{x_{\mathrm{HII}}(1+\delta_b)} \approx 0$. Guided by these arguments, it is sufficient to take the upper limit of the integration in Eq. (6) to be $z = 35$. Note that this calculation of τ is subject to uncertainties in the cosmological and astrophysical parameters, where the latter are more dominant [82]. Therefore we need to understand and model the astrophysical processes more precisely in order to have more reliable predictions of τ.

In Fig. 1, we show the density-weighted mean x_{HII}, i.e., $\overline{x_{\mathrm{HII}}.(1+\delta_b)}$ along with $\overline{x_{\mathrm{HII}}}$, calculated from 21cmFAST. Both quantities increase rapidly below $z \sim 10$ and tend to approach ~ 1 at low redshifts. Although at high redshifts ($z > 14$), $\overline{x_{\mathrm{HII}}.(1+\delta_b)}$ and $\overline{x_{\mathrm{HII}}}$ seem to overlap, we see that they are very different at $z < 14$. In fact, $\overline{x_{\mathrm{HII}}}$ remains below $\overline{x_{\mathrm{HII}}.(1+\delta_b)}$ in the range $z < 14$. This suggests that if we calculate τ based on $\overline{x_{\mathrm{HII}}}$ alone, we will underpredict the τ value.
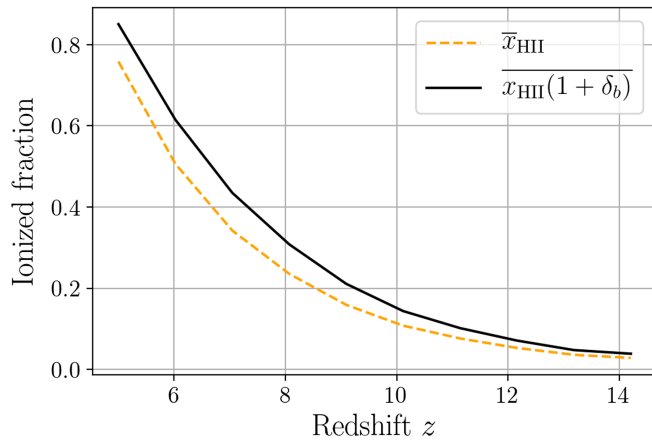

FIG. 1. The density-weighted ionized fraction $\overline{x_{\mathrm{HII}}(1+\delta_b)}$, together with the mean ionized fraction $\overline{x_{\mathrm{HII}}}$, calculated using the corresponding density and ionized fields generated by the 21cmFAST simulations considering Scenario A-I for the astrophysics model, mentioned in Sec. II B. Note here that, $\overline{x_{\mathrm{HII}}(1+\delta_b)}$ and $\overline{x_{\mathrm{HII}}}$ are very different at low redshifts.

D. Computing τ from 21-cm observations

The 21-cm power spectrum is very sensitive to this combination $x_{\mathrm{HII}}(1+\delta_b)$, as can be seen from Eq. (2). However, $x_{\mathrm{HII}}(1+\delta_b)$ cannot be inferred directly from the 21-cm observations. The 21-cm power spectrum probes a complicated combination of $x_{\mathrm{HII}}(1+\delta_b)$ and astrophysics (through T_s) and this introduces degeneracy. Therefore, we not only need a very precise measurement of the 21-cm signal, we also need to have very accurate modeling of the astrophysics in order to use the power spectrum to probe τ. In order to extract $x_{\mathrm{HII}}(1+\delta_b)$ from the 21-cm power spectrum, we use the 21cmFAST seminumerical code. We use the code to compute the quantity $\overline{x_{\mathrm{HII}}(1+\delta_b)}$ in a light-cone box, and integrate it in redshift to get the desired τ. Note that, the choice of reionization process is important here as it decides the sign of the correlation between x_{HII} and δ_b, and here we assume an inside-out model of reionization.

We now briefly outline the process to determine τ in an actual scenario where the 21-cm power spectrum is measured with high confidence from any 21-cm observations. Given a measured 21-cm power spectrum, one can use the 21cmFAST code in a Bayesian inference pipeline to simultaneously fit for the astrophysical and cosmological parameters. Priors on the cosmological parameters can be drawn from CMB or any other observations that measure these parameters more precisely. Once the parameters are determined with confidence, the 21cmFAST code can be run to determine $\overline{x_{\mathrm{HII}}(1+\delta_b)}$ and calculate τ. Since we are using mock data, in order to simplify the analysis we use an equivalent Fisher formalism that basically mimics the above steps. We discuss the Fisher formalism below.

E. Degeneracy between τ and model parameters from 21-cm observations

In this section, we discuss the degeneracy between τ and other parameters, both astrophysical and cosmological. It is important to study the degeneracy in order to understand the improvements on $\Delta \sum m_\nu$ due to 21-cm observations. The fact that CMB or any other probe of cosmological parameters will have different $\tau - \sum m_\nu$ degeneracy in comparison to the 21-cm observations, helps reduce $\Delta \sum m_\nu$. We follow Ref. [81] and explain the process briefly below. Unless otherwise indicated, the results presented here are primarily based on Scenario A.

We define $\tau(\mathbf{p})_{\mathrm{sim}}$ as a function of 11 parameters $\mathbf{p} = [h, \Omega_b h^2, \Omega_c h^2, \ln(10^{10} A_s), n_s, \log L_X, \log f_{\star,10}, \log f_{\mathrm{esc},10}, \log L_{X,\mathrm{mini}}, \log f_{\star,7}, \log f_{\mathrm{esc},7}]$, and given a set of parameter values, $\tau(\mathbf{p})_{\mathrm{sim}}$ yields the value τ from simulation. Note that, the 21cmFAST simulation allows many more parameters that one can vary in order to calculate τ. However, the inclusion of all the parameters makes the analysis lengthy. Furthermore, some parameters do not change the τ values significantly even when varied over a significantly large

range. Based on these considerations, we have chosen the above parameters to study the degeneracies. For more details about the astrophysical parameters, the reader is referred to Refs. [88,89].

$$
\begin{aligned}
\tau_{\text{sim}} \approx 0.056 &+ 0.18\left(\frac{\Delta h}{0.6766}\right) + 0.019\left(\frac{\Delta\Omega_b h^2}{0.02242}\right) + 0.163\left(\frac{\Delta\Omega_c h^2}{0.11933}\right) + 0.12\left(\frac{\Delta\ln(10^{10}A_s)}{3.047}\right) + 0.19\left(\frac{\Delta n_s}{0.9665}\right) \\
&+ 0.0065\left(\frac{\Delta\log L_X}{39.0}\right) - 0.043\left(\frac{\Delta\log f_{\star,10}}{-1.45}\right) - 0.047\left(\frac{\Delta\log f_{\text{esc},10}}{-1.42}\right) + 0.00043\left(\frac{\Delta\log L_{X,\text{mini}}}{39.0}\right) \\
&- 0.033\left(\frac{\Delta\log f_{\star,7}}{-3.0}\right) - 0.016\left(\frac{\Delta\log f_{\text{esc},7}}{-1.42}\right).
\end{aligned}
\tag{7}
$$

Note that, Δp does not denote the uncertainties in the parameters. Rather, it can be treated as a small perturbation around the fiducial values in order to obtain the linearized relation. We have chosen fiducial values such that those produce the best-fit τ value measured by the Planck dataset as discussed in Sec. II A. As mentioned in Ref. [81], this is needed for the self-consistency of the 21-cm predicted τ and the CMB optical depth, which we shall discuss next. From Eq. (7), it can be seen that the coefficients of the linearized equation for the astrophysical parameters are pretty small, and almost an order of magnitude smaller compared to the coefficients of some of the cosmological parameters. The cosmological parameters, on the other hand, have large degeneracies with τ. Note that the coefficients of the linearized relation change to some extent with a change in the fiducial values of the parameters. However, this effect is not huge and the conclusions remain qualitatively the same. The above statements also hold true for Scenarios B and C.

F. Elimination of τ using 21-cm observations

We again emphasize the goal of this work, which is to constrain τ using 21-cm observations and obtain tighter constraints on cosmological parameters like $\Delta\sum m_\nu$. In order to do so, we may perform the following likelihood analysis where we incorporate τ as estimated from the 21-cm observations into the constraints on the parameter set $\mathbf{p}$ by performing a constrained marginalization over τ to obtain a likelihood function $\mathcal{L}(\mathbf{p})$. The likelihood function for such an analysis can be written as

$$
\mathcal{L}(\mathbf{p}) = \int d\tau \mathcal{L}_{\text{expt}}(\mathbf{p},\tau)\mathcal{P}(\tau(\mathbf{p})),
\tag{8}
$$

where $\mathcal{L}_{\text{expt}}$ is the likelihood function from different experiments, which may include CMB, galaxy surveys, 21-cm intensity mapping etc. The probability distribution, $\mathcal{P}(\tau(\mathbf{p}))$, acounts for the modeling/simulations uncertainties on τ. For simplicity, following Ref. [81], we assume $\mathcal{P}(\tau(\mathbf{p}))$ is a Dirac delta function $\delta^D(\tau_{\text{sim}}(\mathbf{p}) - \tau)$. This

choice ensures that the inferred value for τ is consistent with the one predicted by inputting all the other cosmological parameters into the simulations.

Note that the usual analysis would start with a prediction of τ from 21-cm observations, and then use it in the CMB analysis to reduce the uncertainties on the cosmological parameters. But since τ depends on the cosmological parameters [as can be seen from Eq. (7)], the uncertainties can be reduced further using this fact. To include all the information in our Fisher analysis, following Refs. [81,132], we assume that τ values measured from CMB and predicted by 21-cm observations match.

We can thus simplify the likelihood $\mathcal{L}_{\text{expt}}$

$$
\begin{aligned}
\mathcal{L}_{\text{expt}}(\mathbf{p},\tau) \propto \exp\bigg[-\frac{1}{2}\bigg(&F_{\tau\tau}(\Delta\tau)^2 + \sum_{i\neq\tau}F_{i\tau}\Delta p_i\Delta\tau \\
&+ \sum_{j\neq\tau}F_{\tau j}\Delta p_j\Delta\tau + \sum_{ij\neq\tau}F_{ij}\Delta p_i\Delta p_j\bigg)\bigg],
\end{aligned}
\tag{9}
$$

by assuming that it is a multivariate Gaussian distribution with the correlations given by the components of the Fisher matrices calculated for the various observations. Here Δp_i and $\Delta\tau$ are the deviations of ith parameter and τ around their fiducial values [as stated in Eq. (7)], and $F_{ij}, F_{i\tau}, F_{\tau\tau}$ are elements of the Fisher matrix $\mathbf{F}$. For CMB observations with Planck, $\mathbf{F}$ is just the inverse Planck covariance matrix. We sum this with the calculated Fisher matrix for the 21-cm power spectrum using 21cmFAST, assuming the noise and foregrounds expected for observations with HERA. Now we can evaluate the integral in Eq. (8), which is equivalent to substituting τ with $\tau_{\text{sim}}(\mathbf{p})$ in Eq. (9). Using the linear approximation to $\tau_{\text{sim}}(\mathbf{p})$, we then get

$$
\Delta\tau = \sum_i a_i\Delta p_i,
\tag{10}
$$

where a_i are the coefficients that match our linearized relation. Substituting this into Eq. (9) gives us another Gaussian likelihood for $\mathcal{L}(\mathbf{p})$ with modified Fisher matrix

$$F'_{ij} = F_{ij} + a_i F_{j\tau} + a_j F_{i\tau} + a_i a_j F_{\tau\tau}. \qquad (11)$$

This Fisher matrix forms the basis of our analysis, where the information on τ from the 21-cm power spectrum enters as the coefficients a_i. We can now use this modified Fisher matrix to forecast constraints on the parameters.

III. RESULTS

A. Parameter uncertainties with 21-cm estimated τ

Based on the likelihood function, Eq. (9), and the Fisher matrix in Eq. (11), derived in the previous section, we now proceed to make some quantitative predictions.

As mentioned previously, the 21cmFAST code has a number of astrophysical model parameters. When we include MCGs in our calculations (Scenario A), the number of astrophysical parameters almost doubles in comparison to simulations where only ACGs exist. However, we find that parameters for MCGs do not change the τ value considerably even when varied over a large range. Also, the fiducial values for these parameters are largely unknown at high redshifts. Based on these, we consider three cases under Scenario A. Scenario A-I: In this case, we vary the ACG parameters $L_X, f_{\star,10}, f_{\rm esc,10}$ along with the cosmological parameters, keeping the MCG parameters $L_{X,\rm mini}, f_{\star,7}, f_{\rm esc,7}$ fixed. Scenario A-II: This is quite the opposite of Scenario A-I. We vary the MCG parameters along with the cosmological parameters, keeping the ACG parameters fixed. Scenario A-III: In this case, we vary both the ACG and MCG parameters. Since Scenario A-III has more astrophysical parameters, at the outset, we expect that any forecast with Scenario A-III is likely going to be worse as compared to Scenario A-I and Scenario A-II.

The top (bottom) portion of Table II contains the 1-σ constraint on the astrophysical parameters (with fiducial values quoted in the second column) for Scenario A-I (Scenario A-II) based on the mock measurement of the 21-cm power spectrum using HERA, as well as constraints that arise from requiring that the parameters self-consistently reproduce τ in semi-analytic simulations, which we shall refer to as the self-consistency requirement from now on. In parentheses are the 1-σ constraints deduced from Scenario A-III for the entire set of astrophysical parameters considered. Comparing the last two columns, we see that the self-consistency requirement barely improves the constraints on the astrophysical parameters. This result is expected and congruous with the findings of Ref. [81]. We also find that the MCG parameters are almost an order of magnitude less constrained compared to ACG parameters. This indicates that the variation in the MCG parameters does not change the 21-cm signal and τ values as much as the ACG parameters. Considering Scenario A-III, we found that the ACG parameters are slightly less constrained compared to Scenario A-I, and the MCG parameter constraints are very

TABLE II. The fiducial values and 1σ errors for the astrophysical parameters. The results are produced by simultaneously constraining the astrophysics and cosmology parameters while imposing Planck "TT, TE, EE + LowE + Lensing + BAO" prior (Sec. II A) on the latter. The "Errors from $P_{21}(k)$" column shows the 1σ forecast from the 21-cm power spectrum measured using HERA (Sec. II B). The last column contains the errors following the self-consistency requirement (see Sec. II F), which demands that the CMB-measured τ matches the value of τ that is predicted from 21-cm observations. The first three rows correspond to the astrophysical parameters for Scenario A-I, while the last three rows correspond to the same for Scenario A-II. Inside the parenthesis of all the rows, we show the results for Scenario A-III. Note that the self-consistency requirement barely improves the constraints on the astrophysics parameters.

Parameter	Fiducial value	Errors from $P_{21}(k)$	+21-cm τ
$\log L_X$....	39.0	± 0.013 (0.013)	± 0.012 (0.013)
$\log f_{\star,10}$..	-1.45	± 0.022 (0.024)	± 0.018 (0.019)
$\log f_{\rm esc,10}$·	-1.42	± 0.018 (0.032)	± 0.018 (0.032)
$\log L_{X,\rm mini}$	39.0	± 0.12 (0.13)	± 0.12 (0.013)
$\log f_{\star,7}$··	-3.0	± 0.18 (0.23)	± 0.18 (0.023)
$\log f_{\rm esc,7}$··	-1.42	± 0.17 (0.20)	± 0.17 (0.020)

close to what we have for Scenario A-II. This is expected as we have more parameters in Scenario A-III as compared to the other two scenarios and this is possibly making the errors larger. However, since the constraints in Scenario A-III are not much different from the other two cases, we shall only consider the results of Scenario A-I and Scenario A-II from here onward.

Considering the same for cosmological parameters in Table III, for Scenario A-I alone, we find that there is a significant improvement in the constraints on some of the parameters when adding the 21-cm power spectrum and

TABLE III. The fiducial values and 1σ constraints on ΛCDM cosmological parameters. The third column shows the errors from the Planck "TT, TE, EE + LowE + Lensing + BAO" dataset (Sec. II A). The fourth column shows the 1σ forecast from the 21-cm power spectrum measured using HERA gc (considering Scenario A-I for the astrophysics model, mentioned in Section II B). The final column contains the errors following the 'self-consistency requirement' (see Sec. II F). The boldfaced entries represent a substantial reduction in error. In the last column, τ is a derived quantity and the corresponding error is written in italics. Note that the self-consistency requirement significantly improves the constraint on A_s.

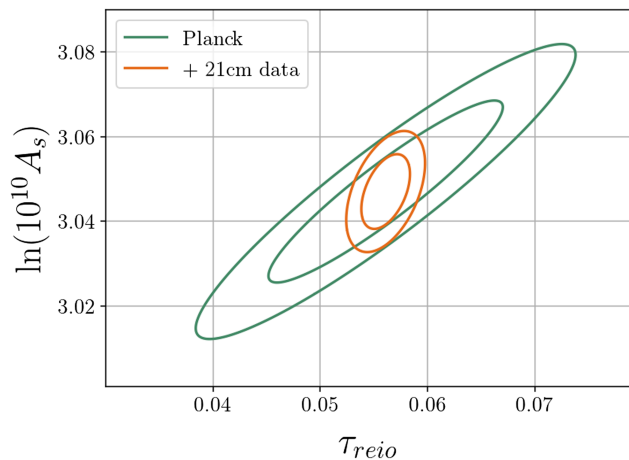| Parameter	Fiducial value	Planck	+$P_{21}(k)$	+21-cm τ
H_0.......	67.66	± 0.42	± 0.15	± 0.15
$\Omega_b h^2$.....	0.02242	± 0.00014	± 0.00012	± 0.00012
$\Omega_c h^2$.....	0.11933	± 0.00093	± 0.00017	± 0.00017
$\ln(10^{10} A_s)$	3.047	± 0.014	± 0.012	$\pm \mathbf{0.0057}$
n_s........	0.9665	± 0.0037	± 0.0028	± 0.0028
τ........	0.056	± 0.0072	± 0.0060	$\pm \mathit{0.0012}$

FIG. 2. The 95% and 68% confidence ellipses in the $\tau -$ $\ln(10^{10}A_s)$ plane. The green contours denote the constraints from Planck "TT, TE, EE + LowE + Lensing + BAO" dataset, while the orange contours are generated after including the 21-cm power spectrum observations from HERA (considering Scenario A-I for the astrophysics model, mentioned in Sec. II B) and the self-consistency requirement on τ (see Sec. II F). We see that the 21-cm observations and the self-consistency requirement together reduce the $\tau - A_s$ degeneracy and also improve the constraints on A_s.

most importantly the self-consistency requirement. We can see, for example, a noticeable reduction in the error bar for $\ln(10^{10}A_s)$, as the 21-cm observations break the CMB degeneracy ($A_s e^{-2\tau}$) between A_s and τ, allowing much better constraints on both parameters. This is evident from Fig. 2, where the 1 and 2σ ellipses on the $A_s - \tau$ plane for Planck shrink and become less tilted when we add information from 21-cm observations. Notice that we had to account for the covariant term between A_s and τ, which was done by considering only the A_s part in Eq. (10) and taking Δp as the 1σ error on A_s. This, of course, is the term determining the tilt of the ellipse. Now considering results for Scenario A-II in Table VI in Appendix B, we see that the cosmological parameter constraints are almost similar for these two scenarios. Based on this finding, from now onward, we shall drop Scenario A-II and mainly focus on Scenario A-I whenever we discuss results for Scenario A.

As mentioned, in the formalism developed in Sec. II F, τ is marginalized out of the set of parameters as a self-consistency requirement. Due to this, in Table III, τ is a measured quantity in the third and fourth columns and appears as a derived quantity in the last column. Now, to estimate the error on the derived τ, we use the likelihood $\mathcal{L}(\mathbf{p})$ given in Eq. (8). We draw random samples of the parameters $\mathbf{p}$ from $\mathcal{L}(\mathbf{p})$, and feed the values into the linearized relation given by Eq. (7) to calculate τ for each set of $\mathbf{p}$. The uncertainty on τ is then estimated from the spread of the τ values. Note that the random drawing process needs to be continued until the standard deviation

of the τ distribution converges. We find that for our calculations, we needed $\mathcal{O}(1000)$ iterations of random drawings before the standard deviation converged. Considering the random drawing of both astrophysical and cosmological parameters in this manner and focusing on Scenario A-I, we find a 1σ error on τ of ±0.0012. It is interesting to check which set among the astrophysical and cosmological parameters yield the maximum error on τ. Suppose we first want to check the effect of the cosmological parameters. To do so, we marginalize Eq. (8) over the astrophysical parameters and obtain $\mathcal{L}(\mathbf{p})$ which now contains only the cosmological parameters. Given this $\mathcal{L}(\mathbf{p})$ in hand, we perform the random drawing of the cosmological parameters. We find that the cosmological parameters yield ±0.00052 error on τ. Repeating the same process for the astrophysical parameters, where the cosmological parameters are marginalized before obtaining the desired $\mathcal{L}(\mathbf{p})$, we find that astrophysical parameters introduce ±0.00060 error on τ. Note that, the error reduces significantly once we drop any one set of parameters. This suggests that there are degeneracies between astrophysical and cosmological parameters, which enhances the error when we consider both sets, and the error is reduced when we fix either set.

B. Improvement on the sum of neutrino masses

In this section, we show how information on τ from 21-cm observations can reduce the uncertainties on the sum of neutrino masses $\sum m_\nu$. Cosmic neutrinos affect both the cosmic expansion and the evolution of density perturbations. In the early Universe, neutrinos are relativistic and behave as radiation. As the Universe cools, they gradually become nonrelativistic and behave like matter. If we consider that the total matter density today has a contribution from nonrelativistic neutrinos, then in the past when neutrinos were relativistic, this contribution was missing. This leads to a later matter-radiation equality when neutrinos were still relativistic. Further, the large thermal velocities of neutrinos allow them to stream out of the dark matter potential wells. As a result, they do not contribute to matter clustering, and the growth of structure is suppressed on scales smaller than their free-streaming scale. This suppression can be mimicked by a lower value of A_s. Hence, the degeneracy between τ and A_s leads to a $\tau - \Sigma m_\nu$ degeneracy.

In order to show how 21-cm observations break $\tau - \Sigma m_\nu$ degeneracy, we repeat the same analysis used to produce the results of Sec. III A, but this time including Σm_ν as an additional cosmological parameter. The results are presented in Fig. 3 and Table IV. For the future CMB-S4 predictions (details provided in Appendix A), we use the multipoles $\ell = 50$ and above. Measurement at these multipoles will be important to break the degeneracy.

Forecasts for the Euclid galaxy survey are generated following Ref. [133]. Here we use the constraints coming
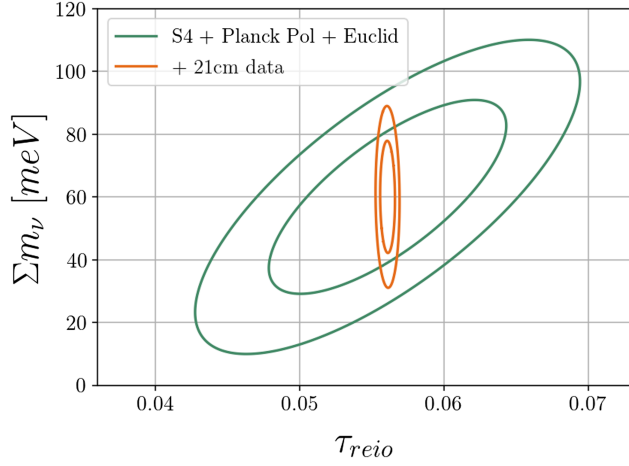
FIG. 3. The 95% and 68% confidence ellipses in the $\tau - \Sigma m_\nu$ plane. The green contours show the results when we combine the Planck polarization measurement at low ℓ, the CMB-S4 forecast at $\ell \geq 50$ and the Euclid galaxy power spectrum forecast. The orange contours show results when, in addition to the data used for the green contours, we combine the 21-cm power spectrum forecast for HERA (considering Scenario A-I for the astrophysics model, mentioned in Sec. II B) and the self-consistency requirement on τ (see Sec. II F). We see that the 21-cm observations and the self-consistency requirement together diminish the $\tau - \Sigma m_\nu$ degeneracy and also improve the constraints on Σm_ν.

only from the galaxy power spectrum. Note that, it is possible to also include the constraints coming from the galaxy bispectrum which will likely help to reduce the parameter errors [133–138]. However, for the current

TABLE IV. The fiducial values and 1σ constraints for the usual ΛCDM cosmological parameters plus the sum of neutrino masses $\sum m_\nu$ as an additional parameter, as discussed in Sec. III B. The third column shows the 1σ errors combining the Planck polarization measurement at low ℓ, forecast from CMB S4 observations at $\ell \geq 50$ and forecast from galaxy power spectrum measured by Euclid survey. The last column shows the 1σ errors when we add forecast for the 21-cm power spectrum measured using HERA (considering Scenario A-I for the astrophysics model, mentioned in Sec. II B) and for the self-consistency requirement, together with the data used to produce results in column three. The boldfaced entries represent a substantial reduction in error. We see that the 21-cm observations together with the self-consistency requirement improve the constraints on $\sum m_\nu$.

| | | $S4_{\ell>50}$ + Euclid | |
Parameter	Fiducial value	+*Planck* Pol	+$P_{21}(k)$ +21 cm τ
H_0............	67.66	± 0.18	± 0.09
$\Omega_b h^2$..........	0.02242	± 0.000031	± 0.000030
$\Omega_c h^2$..........	0.11933	± 0.00032	± 0.00011
$\ln(10^{10} A_s)$.....	3.047	± 0.0078	± 0.0009
n_s.............	0.9665	± 0.0015	± 0.0013
τ.............	0.056	± 0.0043	$\pm \boldsymbol{0.00035}$
$\sum m_\nu$ [meV]...	60	± 16.2	$\pm \boldsymbol{11.8}$

analysis, the forecasts from the galaxy power spectrum are sufficient.

Here, we also include the predictions for the CMB-S4 observations. Note that for the same ℓ range, CMB-S4 observations dominate over Planck. We therefore use the Planck Polarization dataset to avoid any overlap in the ℓ range with CMB-S4. We combine high ℓ CMB-S4 observations with low ℓ Planck Polarization data. This choice automatically avoids any covariance present in the two datasets. Note however that the Planck polarization dataset alone provides a significantly larger error on Σm_ν.

Planck measurement estimated $\Delta \Sigma m_\nu$ to be ± 38 meV using the dataset discussed in Sec. II A. With future CMB-S4 observations at high ℓ, combined with future results from Euclid, it is possible to reduce the 1σ uncertainty down to ± 16.2 meV. Now considering Scenario A-I, when we combine the results from future HERA observations with the self-consistency requirement, we find that the uncertainty on Σm_ν shrinks further down to ± 11.8 meV. This uncertainty is even smaller, ± 6.8 meV, in the case of Scenario A-II, as shown in Table VII in Appendix B. The $\tau - \Sigma m_\nu$ degeneracy breaking due to 21-cm observations can also be seen in Fig. 3 where the tilt of the ellipses becomes vanishingly small as we add information from reionization via the 21-cm observation. The ellipses also shrink, indicating that the degeneracy breaking further improves the constraints on the parameters. In summary, the analysis in this section indicates that it is possible to weigh the neutrinos with $\gtrsim 5\sigma$ accuracy if we combine 21-cm and CMB data. Note, however, that the inclusion of CMB-S4 observations is crucial here as it also helps to break the $\tau - \Sigma m_\nu$ degeneracy and enables a better constraint on Σm_ν. Without CMB-S4 and retaining only the Planck polarization data, the 21-cm observations, and the Euclid survey, the uncertainty in Σm_ν increases up to ± 50 meV.

In addition to the above, we repeat the whole analysis using the observations with Simons Observatory (SO) instead of CMB-S4, and found similar constraints on Σm_ν, as well as on the other parameters. In short, we need to combine the next generation CMB observations along with the 21-cm intensity mapping (and galaxy survey) data in order to achieve better accuracy on Σm_ν.

IV. COMPARING WITH OTHER SCENARIOS

In this section, we compare the results for Scenario A with Scenario B and Scenario C. Note again, that both Scenario B and Scenario C consider only ACGs in the calculations. The only difference is in the parametrization. While Scenario B uses the latest parametrization, Scenario C uses the old parametrization of 21cmFAST [81].

Considering Table V, we find that the ACG parameters for both Scenario A and Scenario B are similarly constrained from the 21-cm observations and the self-consistency requirement improves the constraints only slightly. In the case of Scenario C, the astrophysical parameters are pretty

TABLE V. Same as Table II, but for Scenario B (top rows) and Scenario C (bottom rows).

Parameter	Fiducial value	Errors from $P_{21}(k)$	+21-cm τ
L_X........	39.0	± 0.013	± 0.012
$f_{\star,10}$........	-1.45	± 0.025	± 0.017
$f_{esc,10}$.....	-1.42	± 0.013	± 0.010
ζ..........	30.0	± 1.02	± 1.02
T_{vir} [K]....	8.5×10^4	$\pm 2.21 \times 10^3$	$\pm 2.13 \times 10^3$
R_{mfp} [Mpc]	35	± 6.5	± 6.4

well constrained and the self-consistency requirement makes a small improvement.

Comparing the results with Ref. [81], we find that in our case ζ and T_{vir} are slightly better constrained, and R_{mfp} is slightly less constrained. Note that, we have used 30 redshift bins in the range $z = 5$ to 27. On the other hand, Ref. [81] used a limited redshift range $z \sim 6$ to ~ 10, albeit with many more redshift bins within this range. As we have stated earlier, observations at different redshifts help to break the degeneracy between the different astrophysics parameters and ultimately reduce the uncertainty on the parameters. This is possibly happening with ζ and T_{vir} in our analysis. Now, the parameter R_{mfp} is only important during the reionization. The analysis in Ref. [81] mainly focuses on this z range and has many more z bins than ours on this particular range. Therefore, they have more information on R_{mfp} which helps reduce the uncertainty in R_{mfp} in their analysis.

In Table VIII, we compare the constraints on the cosmological parameters for the three different scenarios of the 21-cm signal modeling. We find that in all the scenarios, the cosmological parameters have similar errors when we add the 21-cm power spectrum observations. For all the scenarios, the self-consistency requirement improves the constraints on A_s significantly, and the constraints on other parameters are improved marginally. Despite this, for each parameter, the constraints look similar in all the scenarios. This is true even for the derived parameter τ, and we find the minimum τ error for Scenario B and maximum for Scenario A-I. Overall, the results in Table VIII suggest that the constraints on the cosmological parameters weakly depend on the detailed modeling of the astrophysics. Note that the constraints can change for different fiducial values of the parameters, although the qualitative results will remain the same.

In Fig. 4 (top), we compare the $\tau - A_s$ degeneracy breaking for the three scenarios mentioned above. Comparing the tilts of the ellipses in the $\tau - A_s$ plane, we see that the tilt is maximum for Scenario A-I, followed by Scenario B, and we find almost no tilt for Scenario C. The errors on τ and A_s are also largest for Scenario A-I. This indicates that, in certain astrophysical scenarios, the $\tau - A_s$ degeneracy cannot be removed fully even with
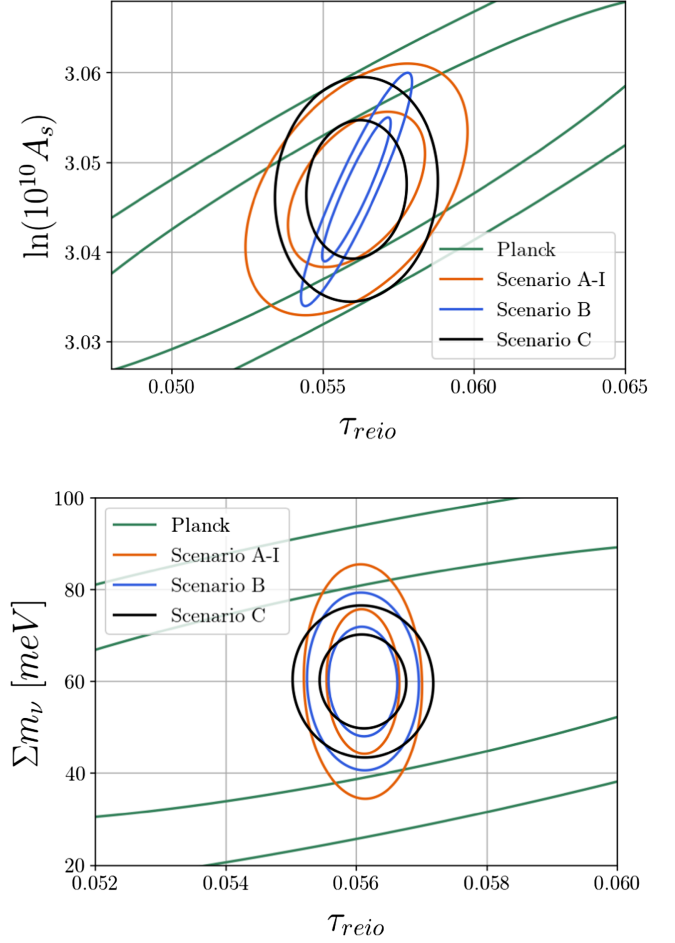

FIG. 4. Top panel is same as Fig. 2 and bottom panel is same as Fig. 3 (bottom). In addition to Scenario A-I, these figures show results for Scenario B and Scenario C. We see that the $\tau - A_s$ degeneracy is minimum for Scenario C. We see that the $\tau - \Sigma m_\nu$ degeneracy is vanishingly small for all scenarios.

information on τ supplied from the 21-cm observations, and the degree of this remaining degeneracy is model dependent.

In Table IX, we compare our results for $\Delta \sum m_\nu$ under the three astrophysical scenarios. In column two of this table, we show predictions for $\Delta \sum m_\nu$ when the Planck polarization (low ℓ) data is analyzed together with CMB-S4 and Euclid data. Note that CMB-S4 is predicted to measure the lower power spectrum multipoles very accurately, which is crucial for the measurement of the reionization bump and this provides an independent estimate of τ. We find that $\Delta \sum m_\nu$ is smallest for Scenario C, followed by Scenario B, and finally we get maximum $\Delta \sum m_\nu$ (± 11.8 [meV]) for Scenario A-I which is slightly better than the result obtained by combining the estimates of the Planck polarization map along with the CMB-S4 and Euclid predictions (± 16.2 [meV]). Although the derived parameter τ has maximum error for Scenario C, the constraints on τ for other scenarios are not far from this

value. These results indicate that the accuracy of the neutrino mass measurement depends very much on the modeling of astrophysics.

In Figure 4 (bottom), we show the $\tau - \Sigma m_\nu$ degeneracies for the three astrophysical scenarios. Comparing the tilt of the ellipses, we can clearly see that the degeneracy is vanishingly small for all three scenarios considered. This suggests that the 21-cm observations can successfully break the degeneracy between τ and Σm_ν, and this result is largely independent of the modeling of astrophysics.

V. SUMMARY AND CONCLUSIONS

Neutrino oscillation experiments have established that neutrinos have nonzero mass, and there is a mass hierarchy for the three flavors of neutrinos. Massive neutrinos change the kinematics of our Universe's expansion. They also dampen structure growth on scales below their free-streaming length, leading to a deficit in power on small scales. This effect is more pronounced if the sum Σm_ν of their masses is large. Neutrinos signatures can be observed in the CMB and galaxy power spectra, and Σm_ν can be constrained using the CMB and large-scale structure observations. This, however, is not straightforward.

The presence of free electrons in the IGM during and after the reionization era limits the cosmological measurement of Σm_ν. Specifically, the optical depth parameter τ, which is a measure of the column density of free electrons in the IGM and one of the ΛCDM model parameters, is degenerate with Σm_ν and the scalar amplitude A_s. This degeneracy hinders the precise measurement of Σm_ν, and also of A_s. We, therefore, need independent and precise estimates of τ from other observations, which can then be used to reduce the uncertainty on Σm_ν. The other option is to measure Σm_ν directly from some observations. This paper focused on the former approach.

The 21-cm signal from reionization is a plausible probe of the IGM electron density, and thus provides an independent measurement of τ. Using it to mitigate the $\tau - \Sigma m_\nu$ degeneracy was first proposed and studied in Ref. [81], which showed that combining 21-cm and CMB data can significantly reduce the uncertainty in Σm_ν (see also Ref. [82], which performs a similar analysis based on cosmological perturbation theory with a symmetries-based bias expansion). In this paper, we revisited this analysis, relaxing sum of the assumptions (such as $T_S \gg T_{CMB}$) and using a modified version of the 21cmFAST code that is interfaced directly with the CMB code CLASS so that the degeneracies between astrophysical and cosmological parameters could be consistently accounted for. We have further considered additional effects like the Lyman-α heating of IGM, Population III stars, the relative velocity between dark matter and baryon fluid, inhomogeneous Lyman-Werner (LW) radiation feedback in our analysis.

We considered 21-cm observations with the HERA radio telescope spanning the range $5 \leq z \leq 27$, in a scenario with moderate foreground contamination (see Ref. [125]). Although the moderate foregrounds plague the 21-cm power spectrum measurement at $z > 20$, we still have significant sensitivity near the reionization redshifts. The power spectrum is then used to constrain the astrophysical model parameters. The current generation of 21-cm observations, like HERA, does not have much sensitivity to constrain the cosmological parameters. Thus, initially, it can be assumed that the cosmological parameters are known from CMB and other observations, and the astrophysical parameters will only be determined from the 21-cm power spectrum. Having the astrophysical parameters in hand, we can use them in a simulation, like 21cmFAST, to generate the density and ionization fields. τ can be estimated from the density-weighted ionization fraction. Finally, this τ value can be used in the CMB analysis to break the $\tau - \Sigma m_\nu$ degeneracy.

Realistically the CMB, 21-cm and other data should be analyzed jointly in Bayesian analysis to predict the astrophysical and cosmological parameters. In this way, the information from the 21-cm observations propagates self-consistently into predicting the τ values in the analysis. However, here we do not perform a joint analysis. Therefore, to achieve this self-consistency, we assume that the CMB predicted τ matches with the τ estimated from the 21-cm power spectrum. Based on this self-consistency requirement, following Ref. [81], we devise a Fisher analysis technique and summarize our main findings below.

We find that the astrophysical parameters can be well constrained with 21-cm observations. Although, parameters associated with the MCGs are less constrained compared to the parameters related to ACGs. MCGs (or Population III stars) do not play a dominant role in the reionization process, so the parameters related to MCGs do not change the τ values noticeably even when changed over a large range. Considering the forecast for the cosmological parameters, we find that the 21-cm derived τ information reduces the uncertainties in all the parameters. This is most significant for A_s, where this mitigates the degeneracy $A_s e^{-2\tau}$ inherent to the CMB. However, this degeneracy breaking depends on the astrophysics models and we found that in certain astrophysical scenarios, this degeneracy is not completely alleviated.

21-cm observations are key for a precise cosmological measurement of the sum of neutrino masses. Future CMB observations promise to measure the reionization bump at low ℓ multipoles of the polarization power spectrum, which can provide an independent measurement of τ and break the $\tau - \Sigma m_\nu$ degeneracy. Meanwhile, future galaxy surveys will provide independent measurements of Σm_ν. Combining estimates for CMB-S4 and Euclid, along with Planck polarization data, we find that Σm_ν can only be measured with a ± 16.2 [meV] error, for a fiducial Σm_ν of 60 [meV] (the minimum value predicted by terrestrial experiments). This uncertainty can be further reduced to ± 11.8 [meV] or lower,

using the 21-cm derived τ information from HERA observations. All this translates into a $\gtrsim 5\sigma$ detection of Σm_ν for the fiducial Σm_ν value and astrophysical models considered.

Our result is marginally more optimistic than that obtained in Ref. [81]. Considering the bounds from the neutrino oscillation experiments [139], the minimum value of Σm_ν is ~ 60 meV for the normal hierarchy and ~ 100 meV for inverted hierarchy. Therefore, our results demonstrate that incorporating 21-cm data will enable a robust determination of the neutrino mass hierarchy.

Our analysis is based on the assumption that the foreground in the 21-cm observations with HERA will be confined within specific parts of the $k_\perp - k_\parallel$ plane and we can avoid those k-modes when computing the 21-cm power spectrum (see Sec. II B). We have considered a moderate foreground contamination scenario where the parameters that define the boundary of the foreground wedge in the $k_\perp - k_\parallel$ plane are set as: $a = 0.05\ h\,\mathrm{Mpc}^{-1}$, $b(z)$ is decided by the horizon limit, and baselines are added coherently. Although, in reality, foregrounds are not so well behaved and in real observations, foregrounds contaminate the $k_\perp - k_\parallel$ space even beyond the expected wedge limit [140,141]. Avoidance of the foreground in such cases results in loss of some or many of the k-modes. A realistic scenario would be to try to clean the contaminated k-modes and recover the cosmological information; this however introduces additional challenges. Adding any realistic foreground scenario is beyond the scope of this work. In order to check the robustness of our results against the assumptions on the foreground, we have considered another scenario where the foreground wedge contaminates a significant amount of the $k_\perp - k_\parallel$ space and we call it a "pessimistic" contamination scenario. Here, the only two modifications over the moderate scenario are that $a = 0.1\ h\,\mathrm{Mpc}^{-1}$ and the baselines are added incoherently. We find that there is a slight increase in uncertainty of $\Delta \Sigma m_\nu$, ± 13.2 [meV], when we consider the pessimistic foregrounds. This is expected as more of the k-modes are now contaminated as compared to the moderate scenario. However, we have sufficient information on τ from the remaining k-modes that Σm_ν can still be measured with good accuracy. When considering a scenario where a larger fraction of k-modes are compromised due to diverse factors, a decline in measurement accuracy can be anticipated. However, as long as we can effectively address and recuperate the affected k-modes, the prospects for accurately measuring both τ and Σm_ν remain promising.

There are a number of probes, like the Lyman-α forest [47–49], Lyman-α emitting galaxies [50–53], the kSZ effect [54–58], etc; that can directly measure τ. Experiments like JWST also probe astrophysics during the pre-reionization era, which again provides ample information on τ [142]. The galaxy surveys [33,61–63], measurement of the expansion rate using distance ladders [59,60], Lyman-α forest surveys [64,65], line-intensity

mapping [66–68], the post-reionization 21-cm signal [69–75], etc., provide direct estimates of Σm_ν. The velocity acoustic oscillations [107,119,143] (originating from the fluctuations in the relative velocity field between dark matter and baryons) are expected to be observed in the 21-cm power spectrum during the cosmic dawn epoch. The phase shift in the velocity acoustic oscillations caused by the supersonic propagation of neutrinos (similar to what is recently constrained from baryon acoustic oscillations [144]) can also provide direct measurement of Σm_ν. All these independent observations can be combined, along with the CMB and 21-cm data, to pinpoint Σm_ν. We shall explore some of these possibilities in future works.

We finally reiterate the essence of this paper, which is that the high-precision measurement of the 21-cm signal from experiments like HERA and SKA will not only lead to a significant improvement in our comprehension of high redshift astrophysics, but also supply invaluable information about cosmology and fundamental physics, such as the sum of neutrino masses.

APPENDIX A: FISHER ANALYSIS FORMALISM FOR CMB-S4

Here we outline the formalism used to calculate the Fisher matrix for CMB-S4 based on Ref. [145]. The CMB power spectra can be written as

$$C_l^{XY} = (4\pi)^2 \int k^2 T_l^X(k) T_l^Y(k) P(k) dk \qquad \text{(A1)}$$

where the indices $X, Y = T, E$ stand for temperature and E-mode polarization respectively, and T_l^X are their transfer functions. We note we haven't considered the lensing potential C_l^{dd} in our analysis for simplicity.

For a set of parameters θ_i for which we want to forecast the errors, we define the Fisher matrix as

$$F_{ij} = \Sigma_l \frac{2l+1}{2} f_{sky} \mathrm{Tr}\left[C_l^{-1} \frac{\partial C_l}{\partial \theta_i} C_l^{-1} \frac{\partial C_l}{\partial \theta_j}\right] \qquad \text{(A2)}$$

where f_{sky} is the covered fraction of sky and the matrix C_l is defined as

$$\begin{pmatrix} \tilde{C}_l^{TT} & C_l^{TE} \\ C_l^{TE} & \tilde{C}_l^{EE} \end{pmatrix}. \qquad (A3)$$

We further define

$$\tilde{C}_l^{TT} = C_l^{TT} + N_l^{TT},$$
$$\tilde{C}_l^{EE} = C_l^{EE} + N_l^{EE} \qquad (A4)$$

where N_l^{XX} are the noise power spectra, given by

$$N_l^{TT} = \Delta_T^2 \exp^{l(l+1)\sigma_b^2},$$
$$N_l^{EE} = 2 \times N_l^{TT}, \qquad (A5)$$

where Δ_T is the temperature sensitivity and $\sigma_b = \theta_{\mathrm{FWHM}}/\sqrt{8\log(2)}$, with the full-width-half-maximum θ_{FWHM}^2 given in radians.

In our analysis we choose the CMB parameters $\theta_i \in \{H_0, \Omega_b h^2, \Omega_c h^2, \ln(10^{10}A_s), n_s, \tau\}$.

APPENDIX B: ADDITIONAL RESULTS

In this section, we present some additional tables that allow a comparison of the results between the different astrophysical scenarios. Tables VI and VII are same as Tables III and IV respectively, but for Scenario A-II. Moreover, Tables VIII and IX exhibit a comparison between Scenario A-I, Scenario B and Scenario C.

TABLE VI. Same quantities as in Table III, here considering Scenario A-II for the astrophysics model (Sec. II B). The boldfaced entries represent a substantial reduction in error.

Parameter	Fiducial value	Planck	$+P_{21}(k)$	$+21$-cm τ
H_0.......	67.66	±0.42	±0.24	±0.24
$\Omega_b h^2$.....	0.02242	±0.00014	±0.00012	±0.00012
$\Omega_c h^2$.....	0.11933	±0.00093	±0.00036	±0.00036
$\ln(10^{10}A_s)$	3.047	±0.014	±0.011	$\pm\mathbf{0.0065}$
n_s........	0.9665	±0.0037	±0.0030	±0.0030
τ........	0.056	±0.0072	±0.0055	$\pm\mathit{\mathbf{0.0018}}$

TABLE VII. Same quantities as in Table IV, here considering Scenario A-II for the astrophysics model (Section II B). The boldfaced entries represent a substantial reduction in error.

Parameter	Fiducial value	$S4_{\ell>50} +$ Euclid $+$ *Planck* Pol	$+P_{21}(k) +21$ cm τ
H_0............	67.66	±0.18	±0.09
$\Omega_b h^2$..........	0.02242	±0.000031	±0.000030
$\Omega_c h^2$..........	0.11933	±0.00032	±0.00014
$\ln(10^{10}A_s)$.....	3.047	±0.0078	±0.0010
n_s............	0.9665	±0.0015	±0.0013
τ.............	0.056	±0.0043	$\pm\mathit{\mathbf{0.00041}}$
$\sum m_\nu$ [meV]...	60	±16.2	$\pm\mathbf{6.8}$

TABLE VIII. Same quantities as in Table III, including a comparison between Scenario A-I, Scenario B and Scenario C. The boldfaced entries represent a substantial reduction in error.

	Fiducial	*Planck*	Scenario A-I		Scenario B		Scenario C	
			$+P_{21}(k)$	$+21$ cm τ	$+P_{21}(k)$	$+21$ cm τ	$+P_{21}(k)$	$+21$ cm τ
Parameters								
H_0........	67.66	±0.42	±0.15	±0.15	±0.13	±0.13	±0.16	±0.16
$\Omega_b h^2$.....	0.02242	±0.00014	±0.00012	±0.00012	$\pm0.0.00012$	±0.00012	±0.00012	±0.00012
$\Omega_c h^2$.....	0.11933	±0.00093	±0.00017	±0.00017	±0.00012	±0.00012	±0.00025	±0.00025
$\ln(10^{10}A_s)$	3.047	±0.014	±0.012	$\pm\mathbf{0.0057}$	±0.012	$\pm\mathbf{0.0053}$	±0.010	$\pm\mathbf{0.0052}$
n_s........	0.9655	±0.0037	±0.0028	±0.0028	±0.0024	±0.0024	±0.0030	±0.0030
τ........	0.056	±0.0072	±0.0060	±0.0012	±0.0062	±0.0007	±0.0052	±0.001

TABLE IX. Same quantities as in Table IV, including a comparison between Scenario A-I, Scenario B and Scenario C.

Parameters	Fiducia value	S4$_{\ell>50}$ + Euclid + *Planck* Pol	Scenario A-I +21-cm data	Scenario B +21-cm data	Scenario C +21-cm data
H_0.........	67.66	± 0.18	± 0.09	± 0.07	± 0.05
$\Omega_b h^2$.......	0.02242	± 0.000031	± 0.000030	± 0.000030	± 0.000030
$\Omega_c h^2$.......	0.11933	± 0.00032	± 0.00011	± 0.00007	± 0.00015
$\ln(10^{10}A_s)$.	3.047	± 0.0078	± 0.0009	± 0.0009	± 0.0009
n_s..........	0.9655	± 0.0015	± 0.0013	± 0.0012	± 0.0011
τ..........	0.056	± 0.0043	± 0.00035	± 0.00036	± 0.00044
$\sum m_\nu$ [meV]	60	± 16.2	± 11.8	± 7.9	± 6.8

[1] E. Gawiser and J. Silk, The cosmic microwave background radiation, Phys. Rep. **333**, 245 (2000).

[2] B. Feng, H. Li, M. z. Li, and X. m. Zhang, Gravitational leptogenesis and its signatures in CMB, Phys. Lett. B **620**, 27 (2005).

[3] A. Challinor, Constraining fundamental physics with the cosmic microwave background, arXiv:astro-ph/0606548.

[4] B. Li, J. D. Barrow, D. F. Mota, and H. Zhao, Testing alternative theories of dark matter with the CMB, Phys. Rev. D **78**, 064021 (2008).

[5] W. Hu, Lecture notes on CMB theory: From nucleosynthesis to recombination, arXiv:0802.3688.

[6] M. Li and X. Zhang, Cosmological *CPT* violating effect on CMB polarization, Phys. Rev. D **78**, 103516 (2008).

[7] G. Gubitosi, L. Pagano, G. Amelino-Camelia, A. Melchiorri, and A. Cooray, A constraint on Planck-scale modifications to electrodynamics with CMB polarization data, J. Cosmol. Astropart. Phys. 08 (2009) 021.

[8] A. Challinor, CMB anisotropy science: A review, IAU Symp. **288**, 42 (2013).

[9] M. A. Fedderke, P. W. Graham, and S. Rajendran, Axion dark matter detection with CMB polarization, Phys. Rev. D **100**, 015040 (2019).

[10] E. Komatsu, New physics from the polarized light of the cosmic microwave background, Nat. Rev. Phys. **4**, 452 (2022).

[11] Y. Fukuda *et al.* (Super-Kamiokande Collaboration), Evidence for oscillation of atmospheric neutrinos, Phys. Rev. Lett. **81**, 1562 (1998).

[12] S. Fukuda *et al.* (Super-Kamiokande Collaboration), Constraints on neutrino oscillations using 1258 days of Super-Kamiokande solar neutrino data, Phys. Rev. Lett. **86**, 5656 (2001).

[13] S. Fukuda *et al.* (Super-Kamiokande Collaboration), Determination of solar neutrino oscillation parameters using 1496 days of Super-Kamiokande I data, Phys. Lett. B **539**, 179 (2002).

[14] M. C. Sanchez *et al.* (Soudan 2 Collaboration), Measurement of the L/E distributions of atmospheric neutrinos in Soudan 2 and their interpretation as neutrino oscillations, Phys. Rev. D **68**, 113004 (2003).

[15] G. Drexlin, Final neutrino oscillation results from LSND and KARMEN, Nucl. Phys. B, Proc. Suppl. **118**, 146 (2003).

[16] T. Araki *et al.* (KamLAND Collaboration), Measurement of neutrino oscillation with KamLAND: Evidence of spectral distortion, Phys. Rev. Lett. **94**, 081801 (2005).

[17] Y. Ashie *et al.* (Super-Kamiokande Collaboration), A measurement of atmospheric neutrino oscillation parameters by SUPER-KAMIOKANDE I, Phys. Rev. D **71**, 112005 (2005).

[18] M. D. Messier, Review of neutrino oscllations experiments, eConf C **060409**, 018 (2006), arXiv:hep-ex/0606013.

[19] D. J. Eisenstein and W. Hu, Power spectra for cold dark matter and its variants, Astrophys. J. **511**, 5 (1997).

[20] J. Lesgourgues and S. Pastor, Massive neutrinos and cosmology, Phys. Rep. **429**, 307 (2006).

[21] J. Brandbyge, S. Hannestad, T. Haugbølle, and Y. Y. Y. Wong, Neutrinos in non-linear structure formation—the effect on halo properties, J. Cosmol. Astropart. Phys. 09 (2010) 014.

[22] F. Marulli, C. Carbone, M. Viel, L. Moscardini, and A. Cimatti, Effects of massive neutrinos on the large-scale structure of the universe, Mon. Not. R. Astron. Soc. **418**, 346 (2011).

[23] W. Hu, D. J. Eisenstein, and M. Tegmark, Weighing neutrinos with galaxy surveys, Phys. Rev. Lett. **80**, 5255 (1998).

[24] O. Elgaroy and O. Lahav, Neutrino masses from cosmological probes, New J. Phys. **7**, 61 (2005).

[25] S. Wang, Z. Haiman, W. Hu, J. Khoury, and M. May, Weighing neutrinos with galaxy cluster surveys, Phys. Rev. Lett. **95**, 011302 (2005).

[26] A. Goobar, S. Hannestad, E. Mortsell, and H. Tu, A new bound on the neutrino mass from the SDSS baryon acoustic peak, J. Cosmol. Astropart. Phys. 06 (2006) 019.

[27] S. Gratton, A. Lewis, and G. Efstathiou, Prospects for constraining neutrino mass using Planck and Lyman-Alpha forest data, Phys. Rev. D **77,** 083507 (2008).

[28] B. A. Reid, L. Verde, R. Jimenez, and O. Mena, Robust neutrino constraints by combining low redshift observations with the CMB, J. Cosmol. Astropart. Phys. 01 (2010) 003.

[29] Z. Pan and L. Knox, Constraints on neutrino mass from cosmic microwave background and large scale structure, Mon. Not. R. Astron. Soc. **454,** 3200 (2015).

[30] R. Allison, P. Caucal, E. Calabrese, J. Dunkley, and T. Louis, Towards a cosmological neutrino mass detection, Phys. Rev. D **92,** 123535 (2015).

[31] K. N. Abazajian and M. Kaplinghat, Neutrino physics from the cosmic microwave background and large-scale structure, Annu. Rev. Nucl. Part. Sci. **66,** 401 (2016).

[32] S. Roy Choudhury and S. Hannestad, Updated results on neutrino mass and mass hierarchy from cosmology with Planck 2018 likelihoods, J. Cosmol. Astropart. Phys. 07 (2020) 037.

[33] M. M. Ivanov, M. Simonović, and M. Zaldarriaga, Cosmological parameters and neutrino masses from the final Planck and full-shape BOSS data, Phys. Rev. D **101,** 083504 (2020).

[34] I. Tanseri, S. Hagstotz, S. Vagnozzi, E. Giusarma, and K. Freese, Updated neutrino mass constraints from galaxy clustering and CMB lensing-galaxy cross-correlation measurements, J. High Energy Astrophys. **36,** 1 (2022).

[35] Z. Sakr, A short review on the latest neutrinos mass and number constraints from cosmological observables, Universe **8,** 284 (2022).

[36] E. Giusarma, M. Gerbino, O. Mena, S. Vagnozzi, S. Ho, and K. Freese, Improvement of cosmological neutrino mass bounds, Phys. Rev. D **94,** 083522 (2016).

[37] S. Vagnozzi, E. Giusarma, O. Mena, K. Freese, M. Gerbino, S. Ho, and M. Lattanzi, Unveiling ν secrets with cosmological data: Neutrino masses and mass hierarchy, Phys. Rev. D **96,** 123503 (2017).

[38] E. Giusarma, S. Vagnozzi, S. Ho, S. Ferraro, K. Freese, R. Kamen-Rubio, and K. B. Luk, Scale-dependent galaxy bias, CMB lensing-galaxy cross-correlation, and neutrino masses, Phys. Rev. D **98,** 123526 (2018).

[39] S. Zaroubi, The epoch of reionization, arXiv:1206.0267.

[40] J. H. Wise, Cosmic reionisation, Contemp. Phys. **60,** 145 (2019).

[41] B. G. Keating and N. Miller, CMB optical depth measurements: Past, present, future, New Astron. Rev. **50,** 184 (2006).

[42] Z. Haiman and L. Knox, Reionization of the intergalactic medium and its effect on the CMB, ASP Conf. Ser. **181,** 227 (1999), arXiv:astro-ph/9902311.

[43] W. Hu, Reionization revisited: Secondary CMB anisotropies and polarization, Astrophys. J. **529,** 12 (2000).

[44] C. L. Reichardt, Observing the epoch of reionization with the cosmic microwave background, arXiv:1511.01117.

[45] A. Kogut et al. (WMAP Collaboration), Wilkinson microwave anisotropy probe (WMAP) first year observations: TE polarization, Astrophys. J. Suppl. Ser. **148,** 161 (2003).

[46] G. Hinshaw et al. (WMAP Collaboration), Nine-Year Wilkinson microwave anisotropy probe (WMAP) observations: Cosmological parameter results, Astrophys. J. Suppl. Ser. **208,** 19 (2013).

[47] J. S. B. Wyithe, A. Loeb, and C. Carilli, Improved constraints on the neutral intergalactic hydrogen surrounding quasars at redshifts z > 6, Astrophys. J. **628,** 575 (2005).

[48] X. H. Fan, M. A. Strauss, R. H. Becker, R. L. White, J. E. Gunn, G. R. Knapp, G. T. Richards, D. P. Schneider, J. Brinkmann, and M. Fukugita, Constraining the evolution of the ionizing background and the epoch of reionization with $\bar{z}^6$ quasars. 2. a sample of 19 quasars, Astron. J. **132,** 117 (2006).

[49] D. H. Weinberg, R. Dave, N. Katz, and J. A. Kollmeier, The Lyman—alpha forest as a cosmological tool, AIP Conf. Proc. **666,** 157 (2003).

[50] S. Malhotra and J. E. Rhoads, Luminosity functions of Lyman-alpha emitters at z = 6.5, and z = 5.7: Evidence against reionization at z = 6, Astrophys. J. Lett. **617,** L5 (2004).

[51] H. Jensen, P. Laursen, G. Mellema, I. T. Iliev, J. Sommer-Larsen, and P. R. Shapiro, On the use of Ly-alpha emitters as probes of reionization, Mon. Not. R. Astron. Soc. **428,** 1366 (2013).

[52] M. Dijkstra, Lyman alpha emitting galaxies as a probe of reionization, Pub. Astron. Soc. Aust. **31,** 40 (2014).

[53] M. Dijkstra, Constraining reionization with Lyman alpha emitting galaxies, arXiv:1511.01218.

[54] C. P. Ma and J. N. Fry, Nonlinear kinetic Sunyaev-Zeldovich effect, Phys. Rev. Lett. **88,** 211301 (2002).

[55] M. McQuinn, S. R. Furlanetto, L. Hernquist, O. Zahn, and M. Zaldarriaga, The kinetic Sunyaev-Zel'dovich effect from reionization, Astrophys. J. **630,** 643 (2005).

[56] H. Park, P. R. Shapiro, E. Komatsu, I. T. Iliev, K. Ahn, and G. Mellema, The kinetic Sunyaev-Zel'dovich effect as a probe of the physics of cosmic reionization: The effect of self-regulated reionization, Astrophys. J. **769,** 93 (2013).

[57] A. Gorce, S. Ilic, M. Douspis, D. Aubert, and M. Langer, Improved constraints on reionisation from CMB observations: A parameterisation of the kSZ effect, Astron. Astrophys. **640,** A90 (2020).

[58] A. Gorce, M. Douspis, and L. Salvati, Retrieving cosmological information from small-scale CMB foregrounds—II. The kinetic Sunyaev Zel'dovich effect, Astron. Astrophys. **662,** A122 (2022).

[59] M. Wyman, D. H. Rudd, R. A. Vanderveld, and W. Hu, Neutrinos help reconcile Planck measurements with the local universe, Phys. Rev. Lett. **112,** 051302 (2014).

[60] A. G. Riess, W. Yuan, L. M. Macri, D. Scolnic, D. Brout, S. Casertano, D. O. Jones, Y. Murakami, L. Breuval, T. G. Brink et al., A comprehensive measurement of the local value of the Hubble constant with 1 km/s/Mpc uncertainty from the Hubble space telescope and the SH0ES Team, Astrophys. J. Lett. **934,** L7 (2022).

[61] F. Villaescusa-Navarro, A. Banerjee, N. Dalal, E. Castorina, R. Scoccimarro, R. Angulo, and D. N. Spergel, The imprint of neutrinos on clustering in redshift-space, Astrophys. J. **861,** 53 (2018).

[62] N. Palanque-Delabrouille, C. Yèche, N. Schöneberg, J. Lesgourgues, M. Walther, S. Chabanier, and E. Armengaud, Hints, neutrino bounds and WDM constraints

from SDSS DR14 Lyman-α and Planck full-survey data, J. Cosmol. Astropart. Phys. 04 (2020) 038.

[63] A. Chudaykin and M. M. Ivanov, Measuring neutrino masses with large-scale structure: Euclid forecast with controlled theoretical error, J. Cosmol. Astropart. Phys. 11 (2019) 034.

[64] N. Palanque-Delabrouille, C. Yèche, J. Lesgourgues, G. Rossi, A. Borde, M. Viel, E. Aubourg, D. Kirkby, J. M. LeGoff, J. Rich et al., Constraint on neutrino masses from SDSS-III/BOSS Lyα forest and other cosmological probes, J. Cosmol. Astropart. Phys. 02 (2015) 045.

[65] J. Baur, Determining the mass of cosmological neutrinos using Lyman-alpha forests, Ph.D. thesis, 2017, https://inspirehep.net/literature/1765226.

[66] A. Moradinezhad Dizgah, G. K. Keating, K. S. Karkare, A. Crites, and S. R. Choudhury, Neutrino properties with ground-based millimeter-wavelength line intensity mapping, Astrophys. J. **926,** 137 (2022).

[67] J. L. Bernal and E. D. Kovetz, Line-intensity mapping: Theory review with a focus on star-formation lines, Astron. Astrophys. Rev. **30,** 5 (2022).

[68] S. Libanore, C. Unal, D. Sarkar, and E. D. Kovetz, Unveiling cosmological information on small scales with line intensity mapping, Phys. Rev. D **106,** 123512 (2022).

[69] F. Villaescusa-Navarro, P. Bull, and M. Viel, Weighing neutrinos with cosmic neutral hydrogen, Astrophys. J. **814,** 146 (2015).

[70] Y. Oyama, K. Kohri, and M. Hazumi, Constraints on the neutrino parameters by future cosmological 21 cm line and precise CMB polarization observations, J. Cosmol. Astropart. Phys. 02 (2016) 008.

[71] A. K. Pal and T. Guha Sarkar, Constraining neutrino mass using the large-scale H i distribution in the post-reionization epoch, Mon. Not. R. Astron. Soc. **459,** 3505 (2016).

[72] D. Sarkar, S. Bharadwaj, and S. Anathpindika, Modelling the post-reionization neutral hydrogen (H i) bias, Mon. Not. R. Astron. Soc. **460,** 4310 (2016).

[73] D. Sarkar and S. Bharadwaj, Modelling redshift space distortion in the post-reionization H i 21-cm power spectrum, Mon. Not. R. Astron. Soc. **476,** 96 (2018).

[74] D. Sarkar and S. Bharadwaj, Redshift-space distortions of the H i 21-cm intensity mapping signal due to the internal motions within galaxies, Mon. Not. R. Astron. Soc. **487,** 5666 (2019).

[75] D. Sarkar, S. Majumdar, and S. Bharadwaj, Modelling the post-reionization neutral hydrogen (HI) 21-cm bispectrum, Mon. Not. R. Astron. Soc. **490,** 2880 (2019).

[76] M. P. van Haarlem, M. W. Wise, A. W. Gunst, G. Heald, J. P. McKean, J. W. T. Hessels, A. G. de Bruyn, R. Nijboer, J. Swinbank, R. Fallows et al., LOFAR: The low-frequency array, Astron. Astrophys. **556,** A2 (2013).

[77] D. R. DeBoer, A. R. Parsons, J. E. Aguirre, P. Alexander, Z. S. Ali, A. P. Beardsley, G. Bernardi, J. D. Bowman, R. F. Bradley, C. L. Carilli et al., Hydrogen epoch of reionization array (HERA), Publ. Astron. Soc. Pac. **129,** 045001 (2017).

[78] G. Paciga, J. Albert, K. Bandura, T. C. Chang, Y. Gupta, C. Hirata, J. Odegova, U. L. Pen, J. B. Peterson, J. Roy et al., A refined foreground-corrected limit on the HI power

spectrum at $z = 8.6$ from the GMRT epoch of reionization experiment, Mon. Not. R. Astron. Soc. **433,** 639 (2013).

[79] R. Ghara, T. R. Choudhury, K. K. Datta, and S. Choudhuri, Imaging the redshifted 21-cm pattern around the first sources during the cosmic dawn using the SKA, Mon. Not. R. Astron. Soc. **464,** 2234 (2017).

[80] J. R. Pritchard, A. Loeb, and J. S. B. Wyithe, Constraining reionization using 21 cm observations in combination with CMB and Lyman-Alpha forest data, Mon. Not. R. Astron. Soc. **408,** 57 (2010).

[81] A. Liu, J. R. Pritchard, R. Allison, A. R. Parsons, U. Seljak, and B. D. Sherwin, Eliminating the optical depth nuisance from the CMB with 21 cm cosmology, Phys. Rev. D **93,** 043013 (2016).

[82] N. Sailer, S. F. Chen, and M. White, Optical depth to reionization from perturbative 21 cm clustering, J. Cosmol. Astropart. Phys. 10 (2022) 007.

[83] J. R. Pritchard and E. Pierpaoli, Constraining massive neutrinos using cosmological 21 cm observations, Phys. Rev. D **78,** 065009 (2008).

[84] K. N. Abazajian et al. (CMB-S4 Collaboration), CMB-S4 science book, first edition, arXiv:1610.02743.

[85] W. L. K. Wu, J. Errard, C. Dvorkin, C. L. Kuo, A. T. Lee, P. McDonald, A. Slosar, and O. Zahn, A guide to designing future ground-based cosmic microwave background experiments, Astrophys. J. **788,** 138 (2014).

[86] A. Mesinger, S. Furlanetto, and R. Cen, 21 cmFAST: A fast, semi-numerical simulation of the high-redshift 21-cm signal, Mon. Not. R. Astron. Soc. **411,** 955 (2011).

[87] J. Park, A. Mesinger, B. Greig, and N. Gillet, Inferring the astrophysics of reionization and cosmic dawn from galaxy luminosity functions and the 21-cm signal, Mon. Not. R. Astron. Soc. **484,** 933 (2019).

[88] Y. Qin, A. Mesinger, J. Park, B. Greig, and J. B. Muñoz, A tale of two sites—I. Inferring the properties of minihalo-hosted galaxies from current observations, Mon. Not. R. Astron. Soc. **495,** 123 (2020).

[89] J. B. Muñoz, Y. Qin, A. Mesinger, S. G. Murray, B. Greig, and C. Mason, The impact of the first galaxies on cosmic dawn and reionization, Mon. Not. R. Astron. Soc. **511,** 3657 (2022).

[90] L. Chuzhoy and P. R. Shapiro, Heating and cooling of the intergalactic medium by resonance photons, Astrophys. J. **655,** 843 (2007).

[91] X. L. Chen and J. Miralda-Escude, The spin—kinetic temperature coupling and the heating rate due to Lyman—alpha scattering before reionization: Predictions for 21 cm emission and absorption, Astrophys. J. **602,** 1 (2004).

[92] A. Oklopčić and C. M. Hirata, Lyα heating of inhomogeneous high-redshift intergalactic medium, Astrophys. J. **779,** 146 (2013).

[93] B. Ciardi, R. Salvaterra, and T. Di Matteo, Lyalpha versus x-ray heating in the high-z IGM, Mon. Not. R. Astron. Soc. **401,** 2635 (2010).

[94] S. Mittal and G. Kulkarni, Ly α coupling and heating at cosmic dawn, Mon. Not. R. Astron. Soc. **503,** 4264 (2021).

[95] B. W. O'Shea and M. L. Norman, Population III star formation in a Lambda CDM universe. 2. Effects of a photodissociating background, Astrophys. J. **673,** 14 (2008).

[96] M. Trenti, Population III star formation during and after the reionization epoch, AIP Conf. Proc. **1294,** 134 (2010).

[97] J. Mirocha, R. H. Mebane, S. R. Furlanetto, K. Singal, and D. Trinh, Unique signatures of Population III stars in the global 21-cm signal, Mon. Not. R. Astron. Soc. **478,** 5591 (2018).

[98] B. Ciardi, E. Scannapieco, F. Stoehr, A. Ferrara, I. T. Iliev, and P. R. Shapiro, The effect of minihaloes on cosmic reionization, Mon. Not. R. Astron. Soc. **366,** 689 (2006).

[99] T. Kimm, H. Katz, M. Haehnelt, J. Rosdahl, J. Devriendt, and A. Slyz, Feedback-regulated star formation and escape of LyC photons from mini-haloes during reionization, Mon. Not. R. Astron. Soc. **466,** 4826 (2017).

[100] A. Fialkov, Supersonic relative velocity between dark matter and baryons: A review, Int. J. Mod. Phys. D **23,** 1430017 (2014).

[101] R. Barkana, The rise of the first stars: Supersonic streaming, radiative feedback, and 21-cm cosmology, Phys. Rep. **645,** 1 (2016).

[102] D. Tseliakhovich and C. Hirata, Relative velocity of dark matter and baryonic fluids and the formation of the first structures, Phys. Rev. D **82,** 083520 (2010).

[103] J. Bovy and C. Dvorkin, Low-mass suppression of the satellite luminosity function due to the supersonic baryon–cold-dark-matter relative velocity, Astrophys. J. **768,** 70 (2013).

[104] A. Stacy, V. Bromm, and A. Loeb, Effect of streaming motion of baryons relative to dark matter on the formation of the first stars, Astrophys. J. Lett. **730,** L1 (2011).

[105] A. Fialkov, R. Barkana, D. Tseliakhovich, and C. M. Hirata, Impact of the relative motion between the dark matter and baryons on the first stars, Mon. Not. R. Astron. Soc. **424,** 1335 (2012).

[106] F. Schmidt, Effect of relative velocity and density perturbations between baryons and dark matter on the clustering of galaxies, Phys. Rev. D **94,** 063508 (2016).

[107] J. B. Muñoz, Robust velocity-induced acoustic oscillations at cosmic dawn, Phys. Rev. D **100,** 063538 (2019).

[108] A. Fialkov, R. Barkana, E. Visbal, D. Tseliakhovich, and C. M. Hirata, The 21-cm signature of the first stars during the Lyman-Werner feedback era, Mon. Not. R. Astron. Soc. **432,** 2909 (2013).

[109] E. Visbal, Z. Haiman, B. Terrazas, G. L. Bryan, and R. Barkana, High-redshift star formation in a time-dependent Lyman–Werner background, Mon. Not. R. Astron. Soc. **445,** 107 (2014).

[110] C. Safranek-Shrader, M. Agarwal, C. Federrath, A. Dubey, M. Milosavljevic, and V. Bromm, Star formation in the first galaxies I: Collapse delayed by Lyman-Werner radiation, Mon. Not. R. Astron. Soc. **426,** 1159 (2012).

[111] M. Ricotti, N. Y. Gnedin, and J. M. Shull, Feedback from galaxy formation: Production and photodissociation of primordial molecular hydrogen, Astrophys. J. **560,** 580 (2001).

[112] Z. Haiman, M. J. Rees, and A. Loeb, Destruction of molecular hydrogen during cosmological reionization, Astrophys. J. **476,** 458 (1997).

[113] K. Ahn, P. R. Shapiro, I. T. Iliev, G. Mellema, and U. L. Pen, The Inhomogeneous Background of Hydrogen-Molecule Dissociating Radiation during Cosmic Reionization, Astrophys. J. **695,** 1430 (2009).

[114] D. Sarkar, J. Flitter, and E. D. Kovetz, Exploring delaying and heating effects on the 21-cm signature of fuzzy dark matter, Phys. Rev. D **105,** 103529 (2022).

[115] J. Lesgourgues, The cosmic linear anisotropy solving system (CLASS) I: Overview, arXiv:1104.2932.

[116] D. Blas, J. Lesgourgues, and T. Tram, The cosmic linear anisotropy solving system (CLASS) II: Approximation schemes, J. Cosmol. Astropart. Phys. 07 (2011) 034.

[117] J. Lesgourgues, The cosmic linear anisotropy solving system (CLASS) III: Comparision with CAMB for LambdaCDM, arXiv:1104.2934.

[118] J. Lesgourgues and T. Tram, The cosmic linear anisotropy solving system (CLASS) IV: Efficient implementation of non-cold relics, J. Cosmol. Astropart. Phys. 09 (2011) 032.

[119] D. Sarkar and E. D. Kovetz, Measuring the cosmic expansion rate using 21-cm velocity acoustic oscillations, Phys. Rev. D **107,** 023524 (2023).

[120] N. Aghanim et al. (Planck Collaboration), Planck 2018 results. I. Overview and the cosmological legacy of Planck, Astron. Astrophys. **641,** A1 (2020).

[121] N. Aghanim et al. (Planck Collaboration), Planck 2018 results. VI. Cosmological parameters, Astron. Astrophys. **641,** A6 (2020); **652,** C4(E) (2021).

[122] P. Madau, A. Meiksin, and M. J. Rees, 21-CM tomography of the intergalactic medium at high redshift, Astrophys. J. **475,** 429 (1997).

[123] R. Barkana and A. Loeb, In the beginning: The First sources of light and the reionization of the Universe, Phys. Rep. **349,** 125 (2001).

[124] S. Bharadwaj and S. S. Ali, On using visibility correlations to probe the HI distribution from the dark ages to the present epoch. 1. Formalism and the expected signal, Mon. Not. R. Astron. Soc. **356,** 1519 (2005).

[125] J. C. Pober, A. R. Parsons, D. R. DeBoer, P. McDonald, M. McQuinn, J. E. Aguirre, Z. Ali, R. F. Bradley, T. C. Chang, and M. F. Morales, The baryon acoustic oscillation broadband and broad-beam array: Design overview and sensitivity forecasts, Astron. J. **145,** 65 (2013).

[126] J. C. Pober, A. Liu, J. S. Dillon, J. E. Aguirre, J. D. Bowman, R. F. Bradley, C. L. Carilli, D. R. DeBoer, J. N. Hewitt, D. C. Jacobs et al., What next-generation 21 cm power spectrum measurements can teach us about the epoch of reionization, Astrophys. J. **782,** 66 (2014).

[127] J. D. Bowman, M. F. Morales, and J. N. Hewitt, Foreground contamination in interferometric measurements of the redshifted 21 cm power spectrum, Astrophys. J. **695,** 183 (2009).

[128] J. S. Dillon, A. Liu, and M. Tegmark, A fast method for power spectrum and foreground analysis for 21 cm cosmology, Phys. Rev. D **87,** 043005 (2013).

[129] B. J. Hazelton, M. F. Morales, and I. S. Sullivan, The fundamental multi-baseline mode-mixing foreground in 21 cm EoR observations, Astrophys. J. **770,** 156 (2013).

[130] A. Liu and M. Tegmark, A method for 21 cm power spectrum estimation in the presence of foregrounds, Phys. Rev. D **83,** 103006 (2011).

[131] A. Datta, J. D. Bowman, and C. L. Carilli, Bright source subtraction requirements for redshifted 21 cm measurements, Astrophys. J. **724**, 526 (2010).

[132] S. Clesse, L. Lopez-Honorez, C. Ringeval, H. Tashiro, and M. H. G. Tytgat, Background reionization history from omniscopes, Phys. Rev. D **86**, 123506 (2012).

[133] V. Yankelevich and C. Porciani, Cosmological information in the redshift-space bispectrum, Mon. Not. R. Astron. Soc. **483**, 2078 (2019).

[134] S. Bharadwaj, A. Mazumdar, and D. Sarkar, Quantifying the redshift space distortion of the bispectrum I: Primordial non-gaussianity, Mon. Not. R. Astron. Soc. **493**, 594 (2020).

[135] A. Mazumdar, S. Bharadwaj, and D. Sarkar, Quantifying the redshift space distortion of the bispectrum II: Induced non-gaussianity at second order perturbation, Mon. Not. R. Astron. Soc. **498**, 3975 (2020).

[136] A. K. Shaw, S. Bharadwaj, D. Sarkar, A. Mazumdar, S. Singh, and S. Majumdar, A fast estimator for quantifying the shape dependence of the 3D bispectrum, J. Cosmol. Astropart. Phys. 12 (2021) 024.

[137] A. Mazumdar, D. Sarkar, and S. Bharadwaj, Quantifying the redshift space distortion of the bispectrum III: Detection prospects of the multipole moments, Mon. Not. R. Astron. Soc. **520**, 2534 (2023).

[138] D. Gualdi and L. Verde, Galaxy redshift-space bispectrum: The importance of being anisotropic, J. Cosmol. Astropart. Phys. 06 (2020) 041.

[139] K. A. Olive et al. (Particle Data Group), Review of particle physics, Chin. Phys. C **38**, 090001 (2014).

[140] A. Liu and M. Tegmark, How well can we measure and understand foregrounds with 21 cm experiments?, Mon. Not. R. Astron. Soc. **419**, 3491 (2012).

[141] G. Bernardi, 21 cm observations: Calibration, strategies, observables, arXiv:1909.11938.

[142] B. E. Robertson, Galaxy formation and reionization: Key unknowns and expected breakthroughs by the James Webb space telescope, arXiv:2110.13160.

[143] J. B. Muñoz, Standard ruler at cosmic dawn, Phys. Rev. Lett. **123**, 131301 (2019).

[144] D. D. Baumann, F. Beutler, R. Flauger, D. R. Green, A. Slosar, M. Vargas-Magaña, B. Wallisch, and C. Yèche, First constraint on the neutrino-induced phase shift in the spectrum of baryon acoustic oscillations, Nat. Phys. **15**, 465 (2019).

[145] J. B. Muñoz, E. D. Kovetz, A. Raccanelli, M. Kamionkowski, and J. Silk, Towards a measurement of the spectral runnings, J. Cosmol. Astropart. Phys. 05 (2017) 032.